

# Investigation of the Microstructural, Mechanical and Corrosion Properties of Grade A Ship Steel-Duplex Stainless Steel Composites Produced *via* Explosive Welding



YAKUP KAYA, NIZAMETTIN KAHRAMAN, AHMET DURGUTLU,  
and BEHÇET GÜLENC

Grade A ship-building steel-AISI 2304 duplex stainless steel composite plates were manufactured *via* explosive welding. The AISI 2304 plates were used to clad the Grade A plates. Optical microscopy studies were conducted on the joining interface for characterization of the manufactured composite plates. Notch impact, tensile-shear, microhardness, bending and twisting tests were carried out to determine the mechanical properties of the composites. In addition, the surfaces of fractured samples were examined by scanning electron microscopy (SEM), and neutral salt spray (NSS) and potentiodynamic polarization tests were performed to examine corrosion behavior. Near the explosion zone, the interface was completely flat, but became wavy as the distance from the explosion zone increased. The notch impact tests indicated that the impact strength of the composites decreased with increasing distance from the explosion zone. The SEM studies detected brittle behavior below the impact transition temperature and ductile behavior above this temperature. Microhardness tests revealed that the hardness values increased with increasing distance from the explosion zone and mechanical tests showed that no visible cracking or separation had occurred on the joining interface. The NSS and potentiodynamic polarization tests determined that the AISI 2304 exhibited higher corrosion resistance than the Grade A steel.

DOI: 10.1007/s11661-017-4161-3

© The Minerals, Metals & Materials Society and ASM International 2017

## I. INTRODUCTION

EXPLOSIVE welding is an effective method of producing multilayered materials which cannot be joined through any other techniques. Bi-metallic transitions are made with a solid-state welding process that uses controlled explosive energy to join two or more otherwise incompatible metals, for example, dissimilar combinations of metals such as copper and magnesium,<sup>[1]</sup> steel and copper,<sup>[2]</sup> steel and titanium,<sup>[3,4]</sup> steel and aluminum,<sup>[5,6]</sup> aluminum and magnesium,<sup>[7,8]</sup> copper and aluminum,<sup>[9,10]</sup> titanium and aluminum,<sup>[11,12]</sup> copper and titanium,<sup>[13]</sup> steel and stainless steel,<sup>[14]</sup> *etc.* Materials produced by explosive welding are widely used in various branches of industry because of their

unique combinations of mechanical and physical properties.<sup>[1]</sup>

A clad steel plate is a composite steel plate obtained by joining stainless steel (cladding metal), *etc.*, to a carbon or low alloy steel (base metal). The most important advantage is that not only is it less costly than similar steels made entirely of cladding materials, but it also provides other features including good mechanical strength and good resistance to heat and corrosion.<sup>[15]</sup>

The yield strength of duplex stainless steel is approximately twice that of standard austenitic stainless steel. Moreover, the pitting resistance, stress corrosion, and corrosion fatigue performance of duplex stainless steel are significantly better than those of conventional austenitic stainless steel.<sup>[16]</sup> Due to their favorable mechanical and corrosion properties, duplex stainless steels are used in a wide range of applications. The higher strength properties allow weight savings, which reduce fabrication costs and enable lighter support structures to be used, and the higher corrosion resistance, in particular against stress corrosion cracking, makes them preferable in certain environments. Therefore, today, the use of duplex stainless steel, consisting

---

YAKUP KAYA and NIZAMETTIN KAHRAMAN are with the Technology Faculty, Karabük University, 78050, Karabük, Turkey. Contact e-mail: ykaya@karabuk.edu.tr AHMET DURGUTLU and BEHÇET GÜLENC are with the Technology Faculty, Gazi University, 06500, Ankara, Turkey.

Manuscript submitted February 15, 2017.

Article published online June 1, 2017

of approximately equal amounts of austenite and ferrite, is established in a wide variety of products, ranging from chemical tankers, pressure vessels and pipes to heat exchangers, paper machines, and offshore applications.<sup>[17]</sup>

Explosive-welded bi-metal transition components provide a solution for corrosion control. Explosive welding is utilized for many industrial processing applications, including those for refineries and chemical plants as well as in the ship-building industry. Ship-building and marine bi-metallic transition joints are one of the oldest applications for explosive welding.<sup>[18]</sup>

Recently, research has been carried out on the fatigue life,<sup>[19]</sup> numerical (smoothed particle hydrodynamic) simulation,<sup>[20]</sup> and physical/experimental modeling<sup>[21]</sup> of explosive-welded bi-metallic composites. Reinforcement of these bi-metallic composites with wire,<sup>[22]</sup> their production from shape-memory alloys<sup>[23]</sup> and multilayer material production<sup>[24]</sup> have also been studied. Much research has been carried out on the production and on the investigation of various aspects of explosive-welded bi-metallic composites. However, the influences of explosion direction (parallel/perpendicular) on the joining interface microstructure and the mechanical properties of these composites have not been dealt with in those studies. In addition, the influence of the distance from the joining interface has not yet been investigated. Neither has any work been seen to deal with the impact transition temperature of these composites nor with the influence of the rolling direction of the base material on the impact transition temperature.

The goal of this study was to manufacture composite plates to be used for offshore and ship-building applications by cladding AISI 2304 duplex stainless steel plates to Grade A ship-building steel plates and to examine the joining capability of the explosive cladding of the Grade A and AISI 2304. The AISI 2304 has better corrosion resistance in sea water and its mechanical properties are also much better than Grade A. The reason for using composite plates instead of a single material was to reduce the cost while effecting better corrosion and wear resistance along with acceptable strength. To this aim, AISI 2304 steel plates were cladded on top of Grade A steel plates using explosive welding. Various tests were carried out on the cladded samples to determine the microstructural, mechanical, and corrosion properties of the joints.

## II. EXPERIMENTAL PROCEDURE

In this study, the parallel arrangement was used for explosive cladding as shown schematically in Figure 1. The chemical compositions of the flyer (AISI 2304) and parent material (Grade A) are given in Table I. Preliminary tests were carried out to determine the optimum explosive welding parameters (Table II). The dimensions of the Grade A and AISI 2304 samples were  $500 \times 250 \times 10$  mm and  $500 \times 250 \times 1$  mm, respectively. The explosive material employed was ELBAR 5 (92 pct ammonium nitrate, 5 pct diesel fuel, and min.

3 pct TNT), supplied in powder form (MKE Barutsan Company, Turkey).

The explosion processes were performed three times for each condition and after explosion, the materials were left to cool in open air. For microstructural, mechanical, and corrosion characterization, samples were cut from various parts of the manufactured Grade A-AISI 2304 composite clad plates using electric discharge machining (EDM) wire. The cut samples were classified depending on the explosion direction (parallel or perpendicular) and the distance from the explosion zone (according to four zones). In addition, another classification was made depending on the rolling direction (parallel or perpendicular) of the Grade A (Figure 2).

For metallographic observations, four groups of the samples were cut from the explosive-clad plates as parallel and perpendicular to the explosion direction and these were mounted in bakelite. The grouping was determined based on the distance from the explosion zone, as shown in Figure 2. These samples were then ground and polished to a  $3 \mu\text{m}$  finish and a 3 pct nital solution in distilled water was used as the enchant. The metallographic examinations of the samples were carried out using a Leica DM 4000M optical microscope. Microhardness measurements of the explosive-clad plates were carried out at various intervals on a Shimadzu HMV microhardness measuring unit using a 500 g load.

Charpy impact test samples were prepared from the explosive-clad composites according to ASTM E 23-98 standard. For comparison purposes, similar samples were also prepared from Grade A steel. As the AISI 2304 was coated on top of the Grade A base material, in order to examine its contribution to the impact toughness, the notches were opened only in the Grade A side of the composites, and the impact tests were then carried out. A 45 deg V notch having a fillet radius of 0.2 mm and a depth of 2 mm was machined into the samples as shown in Figure 3. Charpy impact test samples were brought to the test temperatures using a HUBER CC 805 unit working at a temperature range of 193 K/423 K ( $-80 \text{ }^\circ\text{C}/+150 \text{ }^\circ\text{C}$ ). Charpy impact tests were applied to the samples at various temperatures using a computer-controlled 450 J capacity ZWICK ROELL RKP 450 impact tester. The samples were cut from the plates in directions parallel and perpendicular to the rolling. In addition, the samples were classified into four groups depending on their distance from the explosion zone. Notch impact tests at 253 K, 273 K, and 293 K

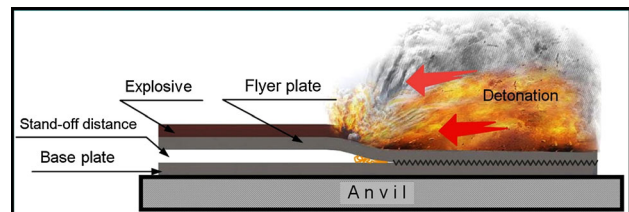


Fig. 1—Parallel arrangement of experimental set up for explosive welding process.

**Table I. The Chemical Composition (Weight Percent) of the Grade A and AISI 2304**

Elements (Wt Pct)	C	Mn	P	S	Si	Al	Cu	Cr	Ni	Mo	Fe
Grade A	0.149	0.7	0.015	0.012	0.166	0.028	0.049	0.022	0.052	0.002	balanced
AISI 2304	0.02	0.10	—	—	—	—	—	23	4.8	0.3	balanced

**Table II. Welding Parameters**

Base Plate	Flayer Plate	Explosive Material	Stand-off Distance	Explosive Rate	Explosive Amount ( $m \times R$ ) (g)
Grade A	AISI 2304	Elbar-5	2t	2.5	2500

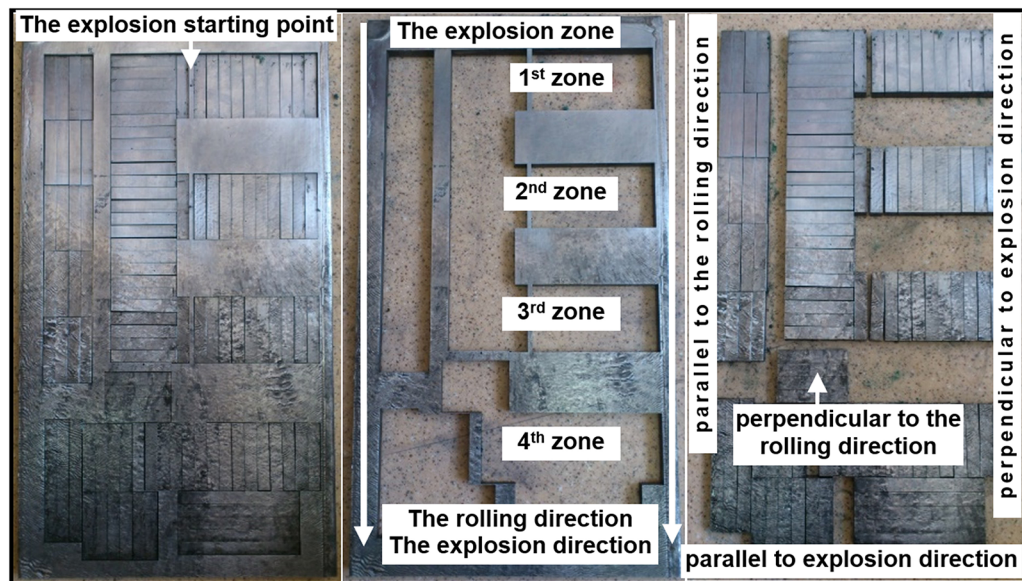


Fig. 2—Pictures of wire EDM cut samples.

( $-20\text{ }^{\circ}\text{C}$ ,  $0\text{ }^{\circ}\text{C}$ , and  $20\text{ }^{\circ}\text{C}$ ) were carried out in order to examine the influence of the distance from the explosion zone on notch impact strength. The fractured surfaces of the samples obtained parallel to the rolling direction over impact transition temperatures were examined using a ZEISS EVO LS10 SEM.

Tensile-shear samples were prepared from the explosive-clad composites both parallel and perpendicular to the explosion direction according to ASTM D 3165-07 (Figure 4). Tensile-shear testing was carried out on a Shimadzu unit with a shear speed of 1 mm/min.

Bending tests of the explosive-clad samples both parallel and perpendicular to the explosion direction were carried out according to ASTM A 263-12 standard. The bending tests were carried out on an Instron unit with a shear speed of 5 mm/min. Samples were again taken from the composite plates both parallel and perpendicular to the explosion direction for the twisting tests.

A neutral salt spray test was applied to each component of the composites individually (Grade A and AISI 2304) with a sea water solution using a SAL 600 TL unit according to ISO 9227. Additionally, the Grade A-AISI 2304 composites were subjected to potentiodynamic polarization tests in 3.5 pct NaCl solution at room

temperature using a Gamry PC4/300 model potentiostat/galvanostat device. After the tests, the surfaces of the samples were examined using a Leica Microscope.

### III. RESULTS AND DISCUSSIONS

#### A. Metallographic Examination

In order to examine the influence of the explosive direction and distance from the explosion zone on the structure of the joining interface, microstructural observation of the Grade A-AISI 2304 composite was carried out on the samples obtained from the composite plates parallel and perpendicular to the explosion direction. Figure 5 presents the microstructural images obtained from a sample perpendicular to the explosion direction, while Figure 6 gives the images obtained from a sample parallel to the explosion direction.

When Figure 5 is examined, a flat, straight interface is seen for the first zone (closest to the explosion zone). As the distance from the explosion zone increases (2nd and 3rd zones), a wavy interface is observed rather than a straight one. At the 4th zone (farthest from the explosion zone), the waviness at the interface increases

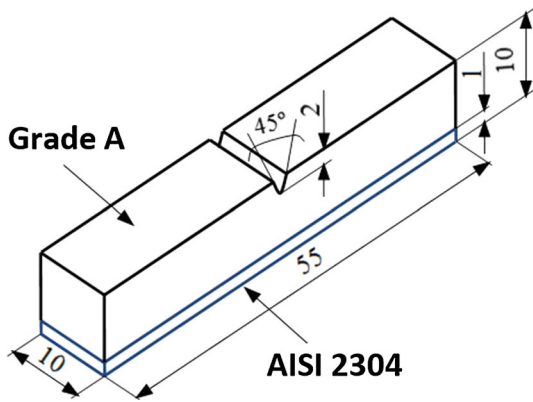


Fig. 3—Charpy impact test samples.

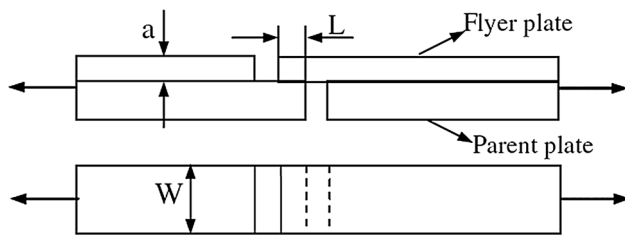


Fig. 4—Schematic representation of tensile-shearing test samples.

significantly. As the distance from the explosion zone increased, the waviness at the interface increased, and thus wave length and amplitude were seen to increase. Additionally, it was determined that the amount of deformation increased with increasing distance from the explosion zone. No work has been published in the literature to date on the influence of distance from the explosion zone on the microstructure. However, some previous studies<sup>[25–27]</sup> have reported that an increasing explosive amount increased collision rate and impact pressure and these, in turn, caused the joining interface to change from a straight form to a wavy one. It was also reported that an increasing explosive amount increased wavelength and amplitude. This present study shows that the effect of increasing distance from the explosion is similar to that of increasing explosive amount.

In addition, Akbari Mousavi and Al-Hassan<sup>[28]</sup> investigated the wavy interface formation in explosive welding. They observed various morphologies in the interface depending on the degree of severity of the velocity distribution across the surfaces of the plates, *i.e.*, the amount of shear deformation and plastic strain. They also reported that greater shear deformation led to greater changes in the morphology of the interface. That is, at low shear deformation, the interfaces were straight, and as shear deformation increased, they were transformed to a wavy shape. A further increase in shear produced regular waves with vortices.

As the explosion starts from the point seen in Figure 2, it influences the coating material perpendicularly at this point. With increasing distance from this starting point, the influence of the explosion becomes

angular instead of perpendicular. As can be seen from the images (Figure 5) taken from the specimens perpendicular to the explosion direction, the joining interface between the base material and coating material is transformed from a straight form into a wavy one as the distance from the explosion zone increases. These joining interface images indicate the increasing amount of deformation with the increasing distance from the explosion zone. (The increasing hardness with increasing distance from the explosion zone is illustrated further on in Figure 13.) This is additional evidence that the amount of deformation increases as the distance from the explosion zone increases.

When the microstructural images in Figure 6 are examined, it is seen that during explosive welding the Grade A mechanically locks with the AISI 2304 clad material with the help of pressure. This waviness and locking increase the joining surface area. Furthermore, small peninsular and island-like Grade A sections are seen in the AISI 2304. These small islands are considered to have detached from the Grade A and dispersed in the AISI 2304 with the intensity of the explosion. According to Zhang *et al.*,<sup>[16]</sup> peninsular and island-like morphologies are attributed to two factors acting simultaneously: the detonation force and the metal vortex flow. An island-like morphology prevails when the detonation force and metal vortex flow are high.

The waviness in the joining interface is generally seen to begin at some distance ahead of the explosion starting point and to increase with increasing distance. This is shown on a macro scale in Figure 2. It can be clearly understood from the microstructure photos (Figure 5) of the specimens taken perpendicular to the explosion direction. However, the microstructure photos (Figure 6) of the specimens taken parallel to the explosion direction clearly show the mechanical locks in peninsular and island forms rather than in waves. The specimen dimensions were limited, making the 250 mm width insufficient for examination; however, examination of the waviness was possible along the 500 mm length.

## B. Charpy Impact Toughness Results

### 1. Notch impact tests at different temperatures

Notch impact test results of Grade A and the Grade A-AISI 2304 composites at various temperatures are given in Figure 7 for both rolling directions. The figure shows that, at all the temperatures, the samples obtained from both materials in the direction parallel to rolling had a higher impact toughness than those obtained in the direction perpendicular to rolling. It has been reported<sup>[29]</sup> that grains of the material elongate along the rolling direction during rolling; therefore, the V-notches of the samples taken parallel to the rolling were found to be larger than those of the samples taken perpendicular to the rolling.

Figure 7 shows that impact toughness increased with increasing temperature for all the samples. The impact transition temperature was determined to be between 233 K to 223 K (−40 °C to −50 °C) for the samples taken parallel to the rolling direction, while it was

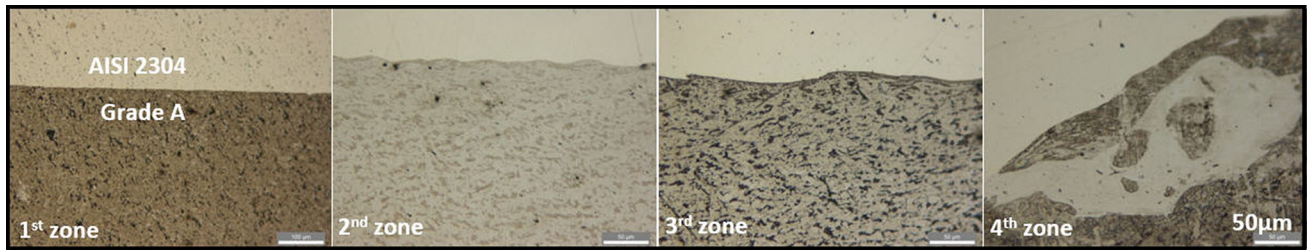


Fig. 5—Joining interface images of the Grade A-AISI 2304 composites (perpendicular to explosion direction).

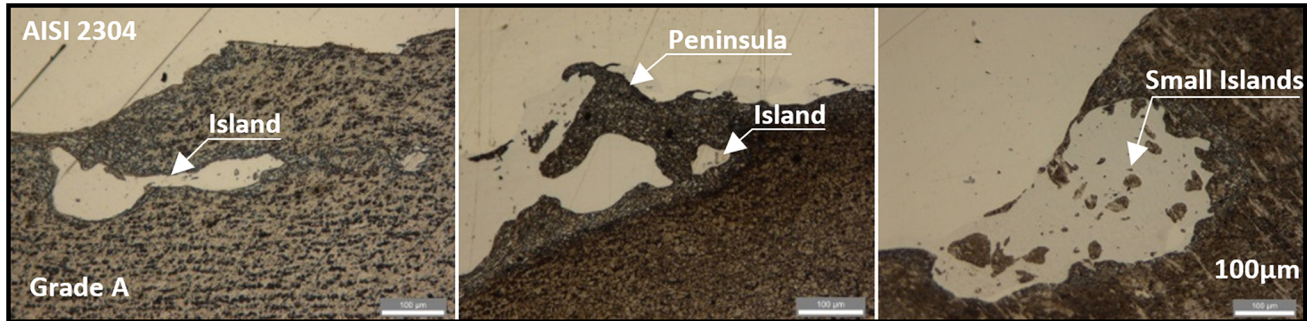


Fig. 6—Joining interface images of the Grade A-AISI 2304 composites (parallel to explosion direction).

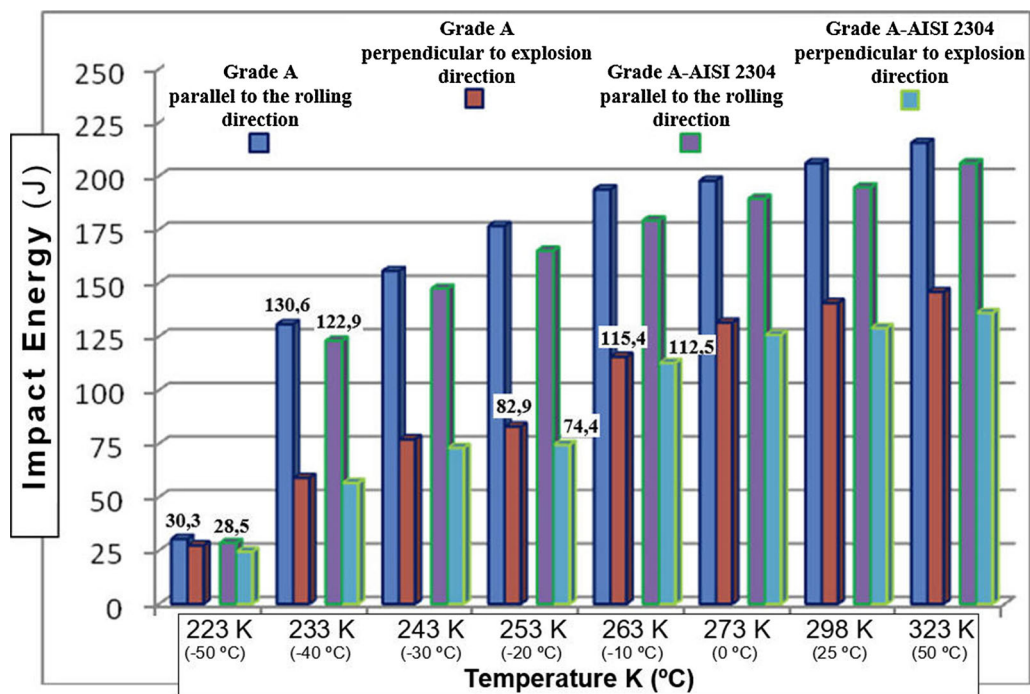


Fig. 7—Notch impact test results of the Grade A and the Grade A-AISI 2304 composites.

between 263 K to 253 K (-10 °C to -20 °C) for the samples taken perpendicular to the rolling direction. Additionally, although the impact toughness differences between the samples taken parallel and perpendicular to the rolling direction were great at high temperatures, there were almost no differences at lower temperatures. One study<sup>[29]</sup> reported that fracture toughness of samples taken parallel to the rolling direction was higher

than that of those taken perpendicular to the rolling direction and that at the same time, the parallel samples showed a higher impact transition temperature than the perpendicular ones. In addition, it was stated that while fracture toughness values of the samples obtained at different rolling directions were quite different from each other at relatively higher temperatures, the difference in fracture toughness values could be disregarded at lower

temperatures. Moreover, the Grade A-AISI 2304 composites were found to exhibit lower impact toughness resistance than the Grade A. This decrease in impact toughness can be attributed to the higher plastic deformation during explosion. In Figure 8, macro images of the samples over impact transition temperatures are given.

In the macro images taken of the samples after notch impact tests, the Grade A and the Grade A side of the Grade A-AISI 2304 composite samples parallel to the rolling direction show ductile behavior up to 233 K (−40 °C) with fractures in the form of tears with fibrous surfaces, while brittle behavior is observed at 223 K (−50 °C) and fracture surfaces are smooth, fine-grained, and shiny without plastic deformation. No separation is seen in any sample. The Grade A and the Grade A side of the Grade A-AISI 2304 composite samples perpendicular to the rolling direction showed an impact transition temperature at between 263 K and 253 K (−10 °C and −20 °C) and started showing brittle fractures after this temperature. In contrast, the Grade A samples perpendicular to the rolling direction (Figure 8(a)) had separated completely at and beyond 233 K (−40 °C) and the Grade A side of Grade A-AISI 2304 composite sample perpendicular to the rolling direction (Figure 8(b)) had fractured. However, the AISI 2304 side of this sample had not separated, though it was bent. Finally, the influence of the rolling direction on impact toughness of the composites was pointed out one more time by taking into account the experimental results along with the literature.

In a similar study, Kaya and Kahraman<sup>[18]</sup> used AISI 316L to clad Grade A *via* explosive welding using various amounts of explosive. They carried out notch impact tests on the clad material and reported that only the Grade A had fractured and the clad material (AISI 316L) was subjected to bending without fracture. Kaçar and Acarer<sup>[14]</sup> clad AISI 316L to P355GH through explosive welding and subjected these explosive-welded materials to impact toughness tests at various temperatures. They also reported that fracture had only taken place in the P355GH and that there was no fracture in the AISI 316L clad material at 296 K, 273 K, and 223 K (25 °C, 0 °C, and −50 °C). In another study of Kaçar and Acarer<sup>[17]</sup> used AISI 2205 to clad P355GH using explosive welding and subjected these explosive-welded materials to impact toughness tests at 296 K, 273 K, and 223 K (25 °C, 0 °C, and −50 °C). As a result, fracture only took place in the P355GH, while the AISI 2205 clad material was bent without fracture at 296 K and 273 K (25 °C and 0 °C). However, the samples had completely fractured at 223 K (−50 °C).

## 2. The influence of distance from explosion zone on impact toughness

Notch impact tests were applied to the Grade A-AISI 2304 composite samples taken parallel to the rolling direction at various temperatures in order to determine the influence of distance from the explosion zone on impact toughness. The notch impact test results are given in Figure 9.

Figure 9 shows that the highest impact toughness of 177.4 J was for the sample from the 1st zone (Figure 2) at 293 K (20 °C), while the lowest impact toughness of 140.2 J was for the sample from the 4th zone at 253 K (−20 °C). At all the temperatures, the impact toughness values of the Grade A-AISI 2304 composites decreased with increasing distance from the explosion zone. As can be seen from the microstructural images in Figure 5, the amount of deformation increased as the distance from the explosion zone increased and this, in turn, increased the waviness in the joining interface. The increasing waviness was considered to result in greater notch effect and this, in turn, decreased the impact toughness. When Figure 9 is examined, depending on the test temperature, the samples obtained from the 4th zone exhibit 140.2 J, 146.5 J, and 154.6 J impact toughness values at 253 K, 273 K, and 293 K (−20 °C, 0 °C and 20 °C), respectively. In all the explosion zones, impact toughness values increased as temperature increased. It has been stated<sup>[30]</sup> that material can fracture with lower energy at lower temperatures, while higher energy is required at higher temperatures to realize fracture. Macro images of the fractured samples at 273 K (0 °C) are given as examples in Figure 10.

After the notch impact tests, ductile fracture was seen for the Grade A-AISI 2304 composites in all the zones at between 253 K and 293 K (−20 °C and 20 °C). It was thought that the samples had been initially subjected to plastic deformation and then fractured. The fractures are seen in tearing mode and the fracture surface is fibrous. As the minimum test temperature was 253 K (−20 °C), impact transition temperature could not be reached and therefore, brittle fracture was not seen.

## C. Fracture Surface SEM Studies

Over the impact transitions temperature, the fracture surfaces of Grade A and the Grade A-AISI 2304 composite samples taken parallel to the rolling direction were examined *via* SEM. The SEM images at different magnifications are shown in Figure 11.

The fracture surface SEM images show the smooth surface resulting from intergranular fracture at 223 K (−50 °C). Furthermore, this fracture is in brittle form with a smooth, shiny surface reflecting the light. At temperatures of 233 K and 243 K (−40 °C and −30 °C) ductile fracture surfaces having a fibrous image are seen. It is believed that micro voids in these surfaces were coalesced and the fracture was in tearing mode (plastic deformation). The SEM results are in agreement with those of previous studies.<sup>[14,17]</sup>

## D. Tensile-Shear Tests

Table III gives the results of tensile-shear tests to which the Grade A-AISI 2304 composite samples taken parallel and perpendicular to the explosion direction were subjected. It is seen from Table III that the composites had higher tensile-shear strength than the original materials of Grade A and AISI 2304. After the tensile-shear tests, no fracture was seen in the joining

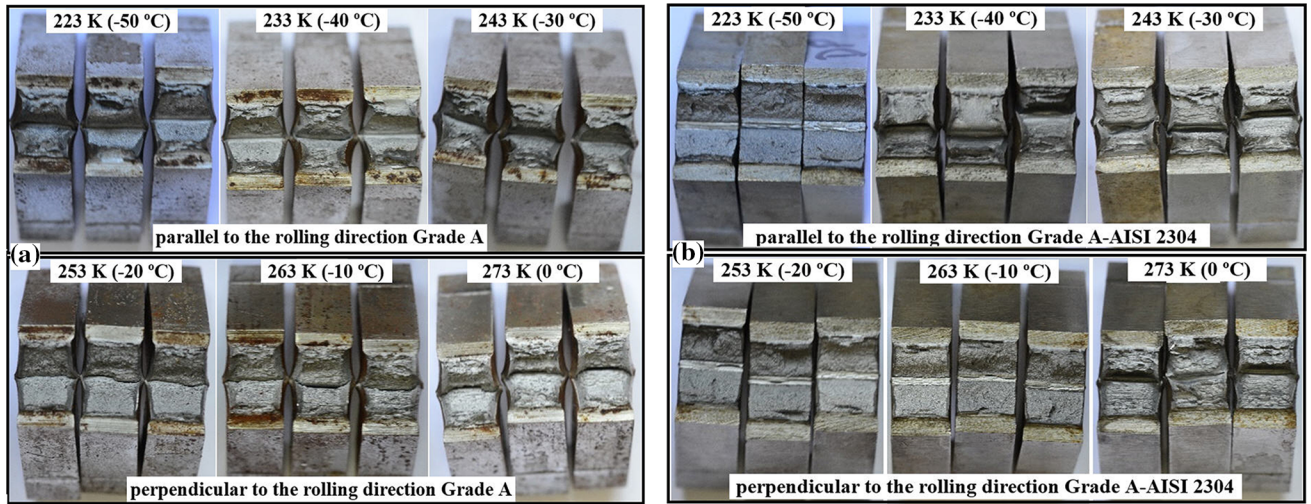


Fig. 8—Macro images of the tested samples over impact transition temperatures (a) the Grade A and (b) the Grade A-AISI 2304 composites.

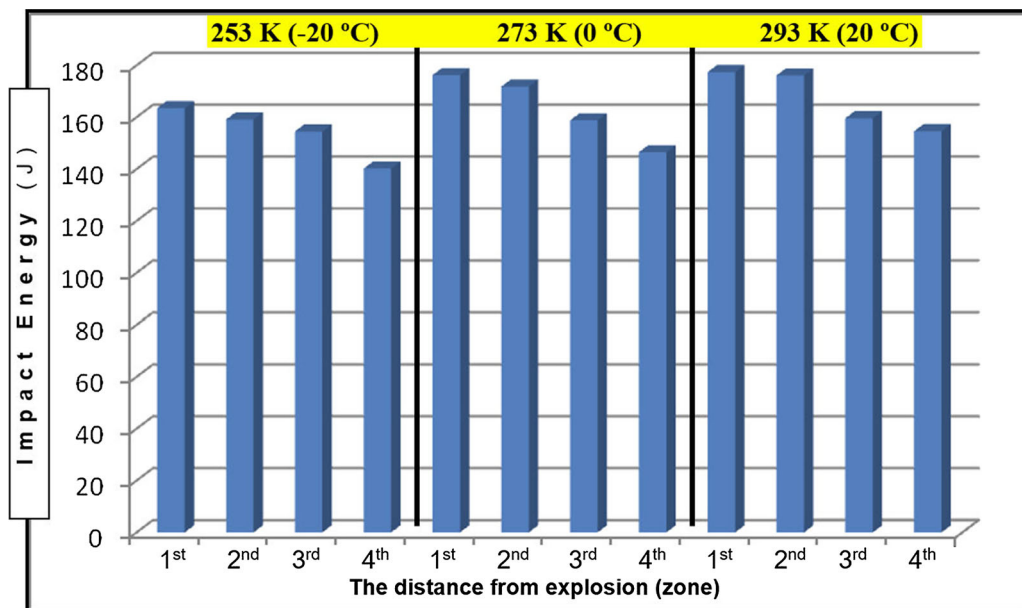


Fig. 9—Notch impact test results of the Grade A-AISI 2304 composites depending on explosion zone.

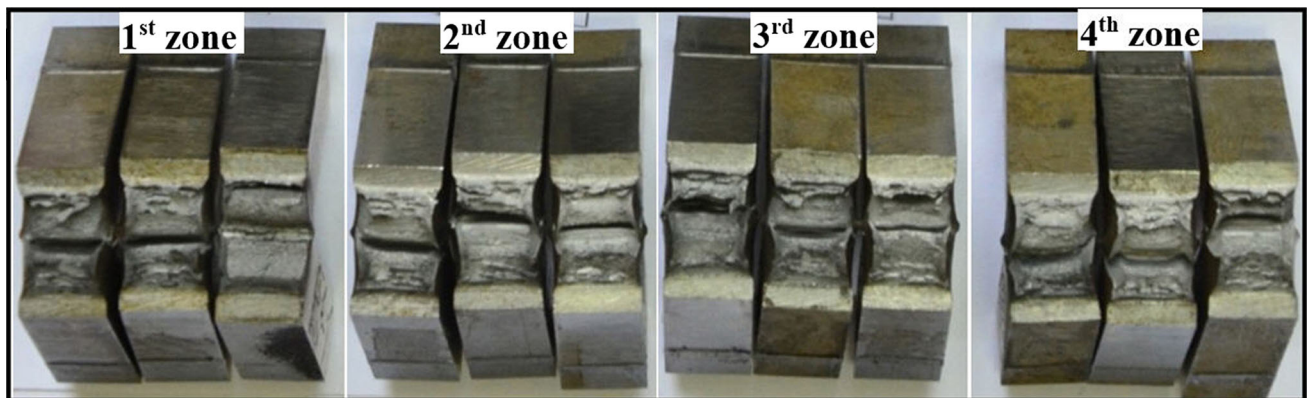


Fig. 10—Macro images of the fractured notch impact test samples at 273 K (0 °C).

interfaces and therefore, the obtained tensile-shear strength was regarded as tensile strength. That the tensile-shear strength of the composites was higher than that of the base metal and clad metal can be attributed to cold deformation during explosion. Other published works have reported that as the amount of cold work applied to metallic materials increases, their tensile strength also increases, due to deformation hardening.<sup>[29]</sup>

When the results were evaluated based on the explosion direction, the sample taken parallel to the explosion direction had a 743.7 N/mm<sup>2</sup> tensile-shear strength and a 27.6 pct elongation. On the other hand, the perpendicular one had a 734.2 N/mm<sup>2</sup> tensile-shear strength and a 23.1 pct elongation. Figure 12 shows that the differences in the strength and elongation values for the composites taken perpendicular to the explosion direction can be explained by the wavy interface structure (Figure 5) which is perpendicular to the tensile-shearing axis. As the wavy structure was perpendicular to the tensile axis, it was thought to cause a notch effect and this effect, in turn, decreased the tensile-shear strength and percent elongation values of the composites.

The fractured tensile-shear samples in Figure 12 show that no separation occurred in the joining interfaces and that fracture took place in the AISI 2304 clad material. Microstructural examinations showed that a wavy structure (Figure 5) was seen in the interface as the distance from the explosion zone increased. This wavy structure increased the surface contact area and caused mechanical locking, with the waves in the Grade A side folding the AISI 2304 (Figure 6). Therefore, no separation in the interface was seen after the tensile-shear tests. These findings indicated that the cladding of AISI 2304 on top of Grade A through explosive welding was performed successfully. Similar successful results were reported in explosion welding of Grade A/AISI 316L, Ti/SS, and Al/Cu by Kaya and Kahraman,<sup>[18]</sup> Kahraman *et al.*,<sup>[31]</sup> and Asemabadi *et al.*,<sup>[32]</sup> respectively.

#### E. Microhardness Tests

Microhardness measurements were carried out on the Grade A-AISI 2304 composite samples in order to determine the influence of distance from the explosion zone on hardness. The results, given in Figure 13, show that the hardness was determined as 372 HV in the 1st zone, 100  $\mu\text{m}$  away from the joining interface, while the original AISI 2304 had a hardness of 242 HV. In the AISI 2304 side, 500 and 900  $\mu\text{m}$  away from the interface, the hardness values were 307 and 307 HV, respectively. In the 2nd zone, the hardness values were 393, 321, and 369 HV for the same distances, respectively. Hardness profiles in the 3rd and 4th zones were also parallel to those in the 2nd zone. Similarly, the measured hardness values in the Grade A side increased with increasing distance from the explosion zone, whereas they decreased with increasing distance from the joining interface. In the mid zone of the Grade A, the hardness values were around 139 HV, very close to the hardness value of the original Grade A. However,

towards the outer side of the Grade A, the hardness started to increase again.

When the hardness results were evaluated, the highest hardness was seen for the joining interface, followed by the outer surfaces and middle areas of the plates. In addition, it was understood that the hardness also increased as the distance from the explosion zone (from 1st zone to 4th zone) increased. In the explosion welding, the joining surfaces and outer surfaces of the plates were subjected to cold deformation. On the other hand, the increasing hardness values with the increasing distance supports the idea that the amount of deformation increases with increasing distance from the explosion zone (see Section III-A). Bina *et al.*<sup>[33]</sup> joined copper and stainless steel using explosive welding and carried out microhardness tests. They reported that the hardness of the samples near the interface was significantly higher than in other parts due to cold deformation and work hardening as the result of the high collision rate during explosion. It was also reported in a study by Bina *et al.* that the hardness of the middle areas of copper and stainless steel plates remained almost unchanged. Yazdani *et al.*<sup>[34]</sup> joined St37 Steel/Ck60 and Hoseini Athar *et al.*<sup>[35]</sup> Al/Cu/Al through explosive welding and they all reported similar results after the microhardness measurements.

#### F. Bending Tests

Bending tests were applied to the Grade A-AISI 2304 composite samples taken parallel and perpendicular to the explosion direction. The tests were carried out in two ways: with the AISI 2304 cladding material held inside and with the AISI 2304 cladding material held outside. Figure 14 shows macro images of the bent samples. After bending up to 180 deg, there was no visible separation, cracking or tearing in the joining interfaces of any of the bent samples. Unlike the tensile-shearing tests, the explosion direction was found to have no effect on the 180 deg bending tests. Moreover, the absence of separation after the bending tests can be attributed to the increasing interface strength due to mechanical locking, as seen in Figure 6.

The absence of any defects in the joining interfaces of the Grade A-AISI 2304 composite samples was an indication of a sound joining and that these composite plates in bent form could be used safely under service conditions. Similar results were reported after bending tests applied to various explosive-welded material couples.<sup>[36–38]</sup>

#### G. Twisting Tests

Macro images of Grade A-AISI 2304 composite samples to which 180 and 360 deg twisting tests were applied are given in Figure 15. The tests were applied to composite samples taken both parallel and perpendicular to the explosion direction. After the tests, there were no visible cracks or tears in the joining interfaces of any of the samples. Thus, the explosion direction (parallel or perpendicular) had no influence on the twisting tests.



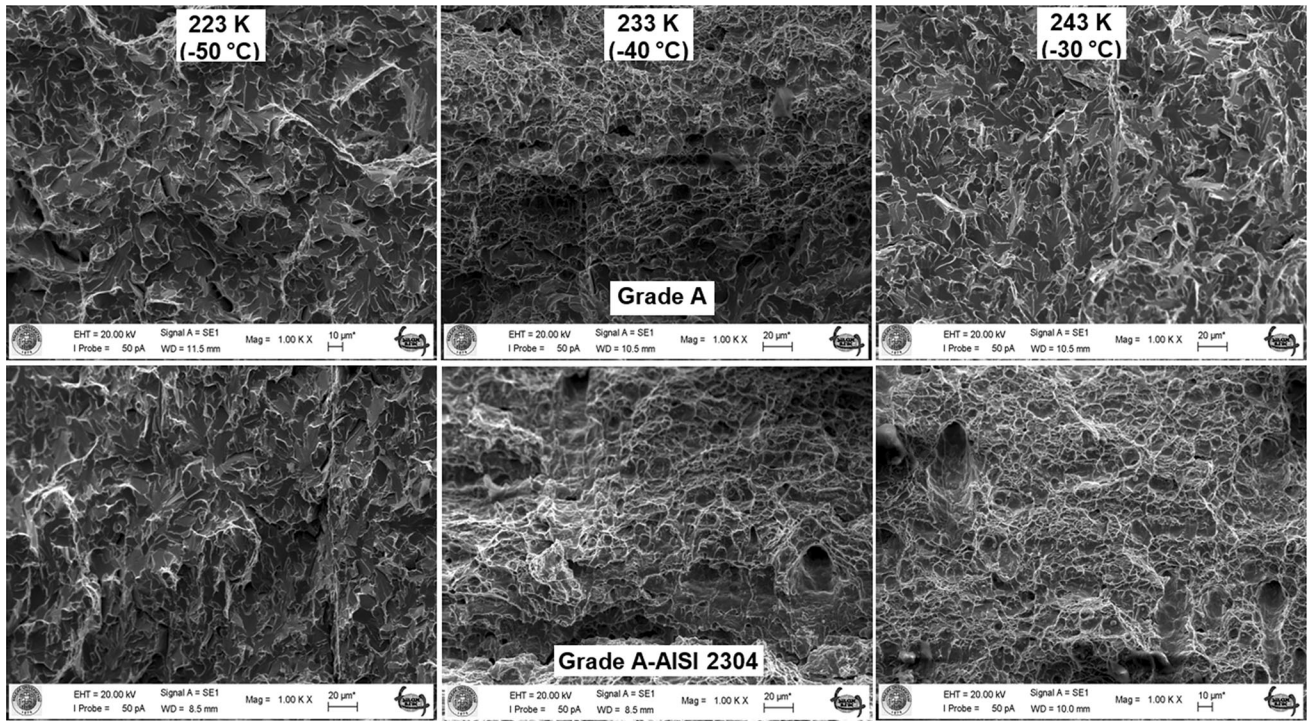


Fig. 11—Fracture surface SEM images of the samples parallel to rolling direction over impact transition temperature.

Table III. Tensile-Shear Test Results

	Grade A (Tensile Strength)	AISI 2304 (Tensile Strength)	Grade A-AISI 2304 Parallel to Explosion Direction	Grade A-AISI 2304 Perpendicular to Explosion Direction
Tensile-shearing strength (N/mm <sup>2</sup> )	430	733	743.7	734.2
Elongation (Pct)	22	37	27.6	23.1

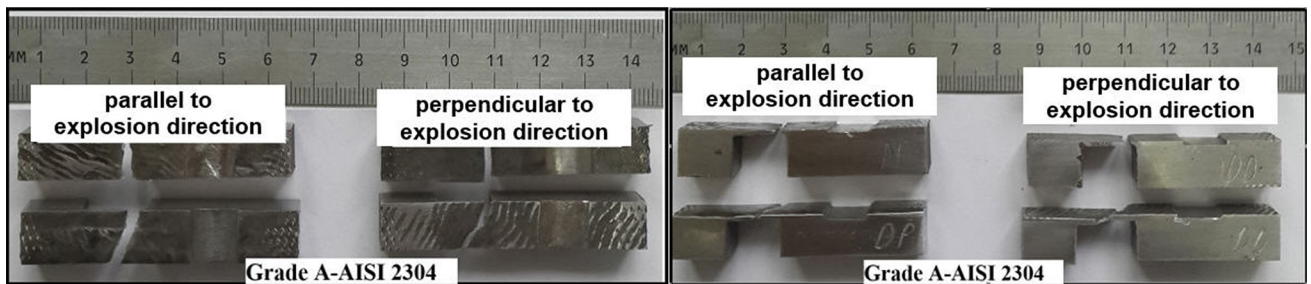


Fig. 12—Macro images of fractured tensile-shearing samples.

After the extreme cold deformation stemming from the explosion pressure during the explosion welding, a secondary deformation was also applied to the explosive-welded samples by the 180 and 360 deg twisting tests. Despite the work hardening effect of these two processes, no cracks or tears were observed on the samples, thus indicating the good quality of the joining at the interface of the samples. The twisting test results showed that the joinings were safe and that these composites could be used in their twisted form in service applications. Wang *et al.*<sup>[38]</sup> carried out twisting tests in order to determine the interface strength of

explosive-welded copper and steel and found the interface strength to be adequate. They also reported that there were no cracks in the interface despite the great deformation and hardening.

#### H. Corrosion Tests

##### 1. Neutral salt spray (NSS) tests

The Grade A and AISI 2304 materials were individually subjected to neutral salt spray tests in sea water in order to examine their corrosion behavior; macro images obtained after the tests are shown in Figure 16.

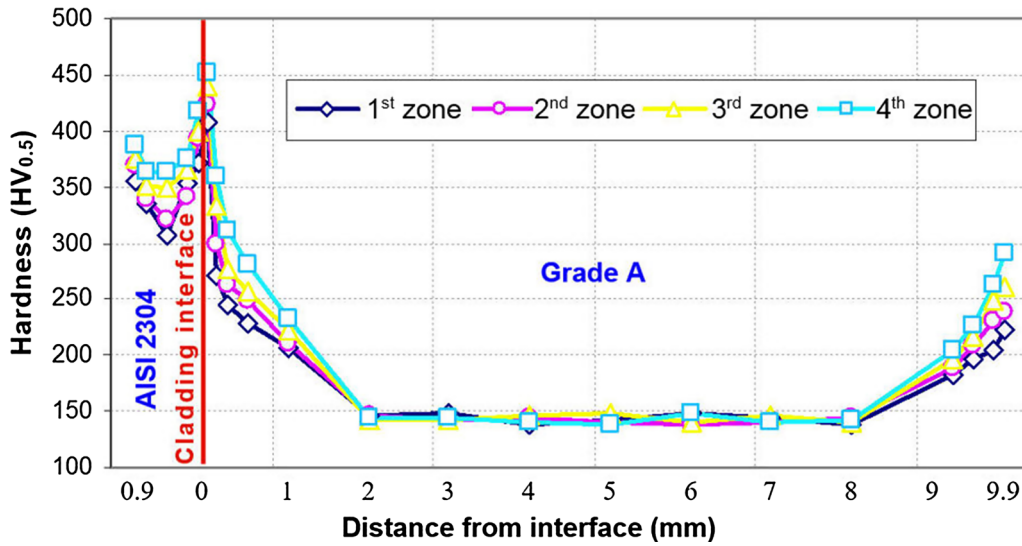


Fig. 13—Hardness results of the Grade A-AISI 2304 composites (depending on the distance from explosion zone).

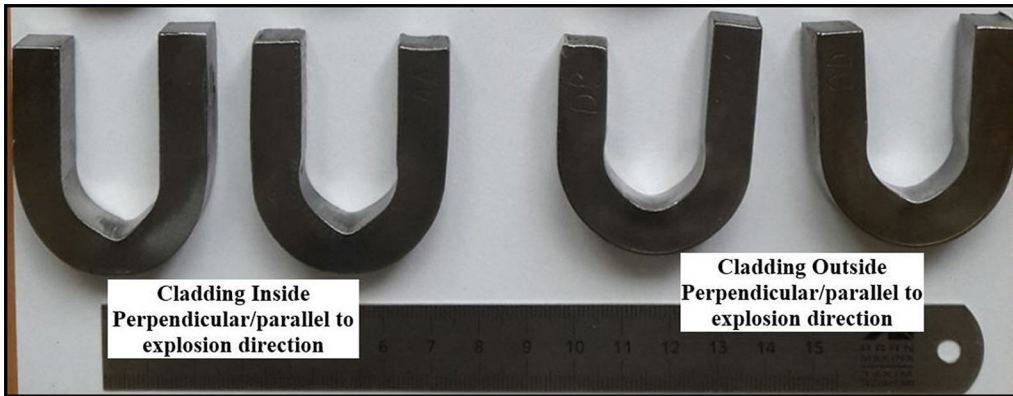


Fig. 14—Macro images of the Grade A-AISI 2304 samples after bending tests.

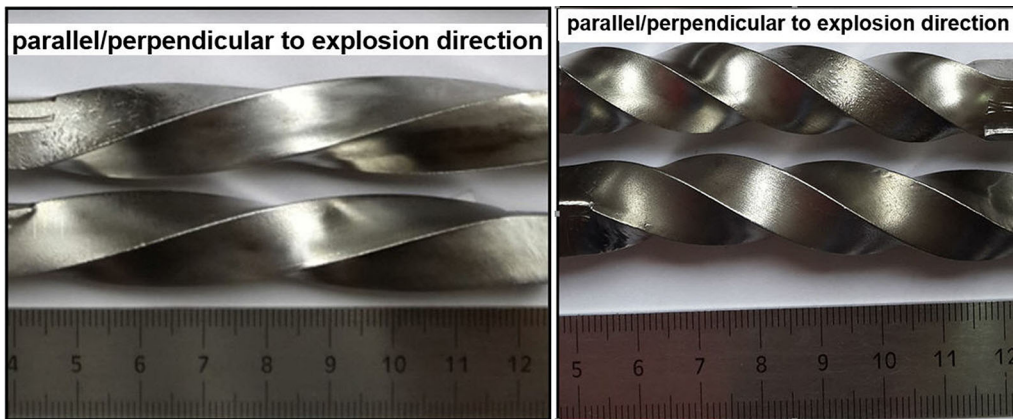


Fig. 15—Macro images of the Grade A-AISI 2304 composite samples subjected to twisting tests.

The images of the samples after the neutral salt spray tests clearly show that the Grade A ship steel had suffered corrosion due to its high chemical affinity with oxygen. After 24 hours, 35 pct of the surface area of the

Grade A material had undergone corrosion. After 48 hours, with the oxidation continuing at the same rate without slowing down, 70 pct of the surface area had become oxidized. In contrast, the rate of corrosion

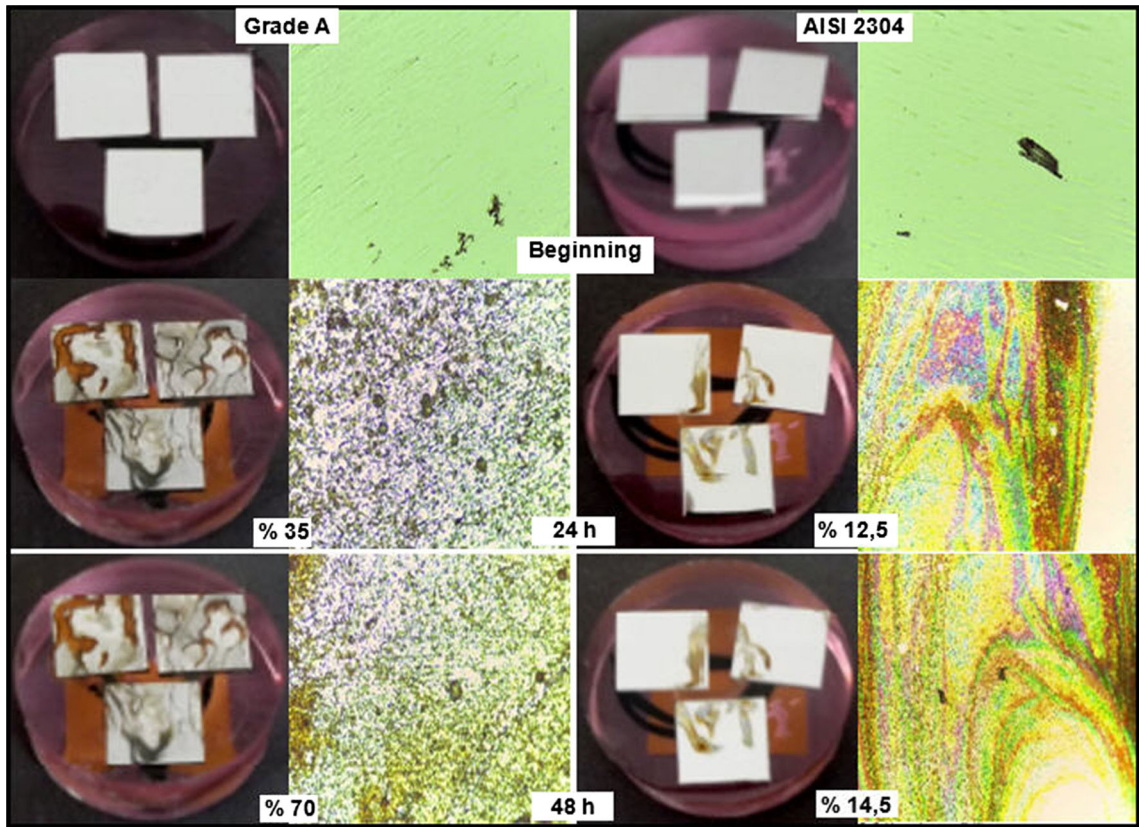


Fig. 16—Macro images of the Grade A and AISI 2304 after neutral salt spray test.

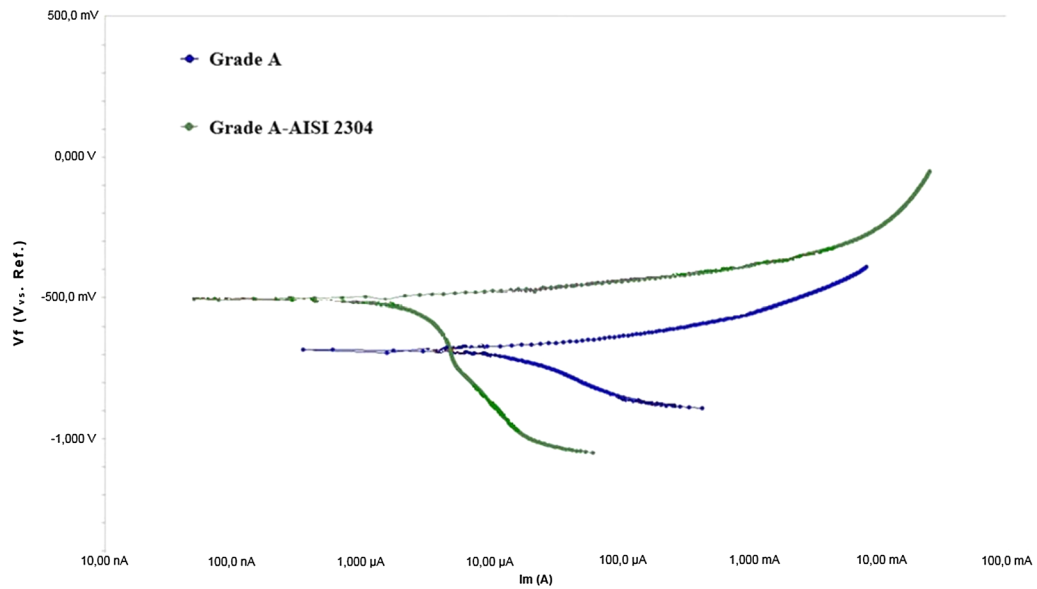


Fig. 17—Polarization test graph of the Grade A-AISI 2304 composite.

for the AISI 2304 duplex stainless steel was very low when compared to that of the Grade A ship steel. After 24 hours, 12.5 pct of the surface area of the AISI 2304 stainless steel had become oxidized. After 48 hours, the oxidation had slowed down and only 14.5 pct of the

surface area had become oxidized. It can be concluded from these neutral salt spray test results that the cladding of AISI 2304 duplex stainless steel on top of Grade A ship steel through explosive welding protects Grade A ship steel against corrosion in a sea water environment.

## 2. Potentiodynamic polarization tests

In order to further examine the corrosion behavior of the Grade A-AISI 2304 composites, potentiodynamic polarization tests were carried out; the obtained results are given in Figure 17.

An evaluation of the potentiodynamic test results showed that the corrosion potential ( $E_{\text{corr}}$ ) value of the Grade A-AISI 2304 composite ( $-504$  mV) was higher than that of the Grade A ( $-687$  mV)  $E_{\text{corr}}$  value, while the corrosion current density ( $I_{\text{corr}}$ ) values of the Grade A ( $33.9 \mu\text{A}$ ) were lower than those of the Grade A-AISI 2304 composite ( $6.57 \mu\text{A}$ ). In potentiodynamic polarization tests, increasing corrosion stress increases the corrosion resistance of a bi-metallic material couple, whereas increasing corrosion current decreases the corrosion resistance. These results showed that, in a sea water environment, the corrosion rate of Grade A was higher than that of the AISI 2304 clad layer of the Grade A-AISI 2304 composites. Results parallel to those obtained in this study can be found in the galvanic corrosion series table in the published literature.<sup>[39]</sup> Acarer<sup>[40]</sup> joined aluminum and copper *via* explosive welding. After electro-chemical corrosion tests were carried out, it was reported that the copper had a higher  $E_{\text{corr}}$  value than the aluminum, but lower  $I_{\text{corr}}$  values and that, according to these results, in sea water, the aluminum of an Al-Cu bi-metallic material couple would be subjected to more galvanic corrosion than the copper.

## IV. CONCLUSIONS

This study examined the microstructural, mechanical, and corrosion properties of Grade A-AISI 2304 composites produced through explosive welding. The following conclusions can be drawn from this present study:

- For the Grade A-AISI 2304 composite samples taken perpendicular to the explosion direction, the completely straight joining interface near the explosion zone was observed to transform into a wavy one with increasing distance from the explosion zone due to increasing cold deformation. Therefore, the wave length and amplitude were seen to increase. However, for the composites taken parallel to the explosion direction, the Grade A wave folding resulted in mechanical locking with the AISI 2304 stainless steel, thereby improving mechanical properties.
- After notch impact tests, higher toughness values were obtained for the Grade A-AISI 2304 composite samples taken parallel to the rolling direction than for those taken perpendicular to it. In addition, the impact toughness values decreased with the increasing amount of deformation as the distance from the explosion zone increased. The SEM examinations of the fractured surfaces showed brittle fractures below the impact transition temperature and ductile fracture above this temperature.
- After the tensile-shear tests, no separation was seen in the joining interfaces of the composite samples,

with those taken parallel to the explosion direction exhibiting higher tensile-shear strength than those taken perpendicular to the explosion direction.

- The highest hardness was obtained for the joining interface, followed by the outer surfaces and middle areas (half the thickness) of the plates. In addition, as the distance from the explosion zone increased, hardness also increased due to the increasing deformation hardening.
- After the 180 deg bending tests were applied to the Grade A-AISI 2304 samples taken parallel and perpendicular to the explosion direction, no separation, cracks, or tearing were visible to the naked eye at the joining interfaces of any of the composites.
- The 180 and 360 deg twisting test results revealed no visible defects in the joining interfaces of any of the composites.
- Neutral salt spray test results showed that the AISI 2304 duplex stainless steel clad on top of the Grade A ship steel plate exhibited higher corrosion resistance than Grade A steel.
- Potentiodynamic polarization test results showed that the galvanic corrosion resistance of the AISI 2304 duplex stainless steel was higher than that of the Grade A steel.
- Results of the experimental studies revealed that the mechanical and corrosion properties of Grade A ship-building steel were improved by explosive welding/cladding with AISI 2304 duplex stainless steel.

## ACKNOWLEDGMENTS

We would like to thank to MKE Barutsan Company, Turkey for kindly supplying the materials, equipment, and staff. This work was financially supported under Karabuk University Project (KBU-BAP-13/1-DR-012).

## REFERENCES

1. M. Kwicien, J. Majta, and D. Dziedzic: *Arch. Civil. Mech. Eng.*, 2014, vol. 14, pp. 32–39.
2. R. Ma, Y. Wang, J. Wu, and M. Duan: *Fusion. Eng. Design*, 2014, vol. 89, pp. 3117–24.
3. T.N. Prasanthi, C. Sudha Ravikiran, and S. Saroja: *Mater. Design*, 2016, vol. 93, pp. 180–93.
4. M. Gloc, M. Wachowski, T. Plocinski, and K. Jan Kurzydowski: *J. Alloys Compd.*, 2016, vol. 671, pp. 446–51.
5. L. Tricarico and R. Spina: *Mater. Design*, 2010, vol. 31, pp. 1981–92.
6. X. Guo, H. Wang, Z. Liu, L. Wang, F. Ma, and J. Tao: *Int. J. Adv. Manuf. Technol.*, 2016, vol. 82, pp. 543–48.
7. I. Samardzic, B. Matesa, and I. Kladaric: *Metallurgija*, 2011, vol. 50 (3), pp. 159–62.
8. V.N. Arisova, Y.P. Trykov, I.A. Ponomareva, and E.V. Miroshnikova: *Rus. J. Non-Ferrous Metals*, 2014, vol. 55 (1), pp. 46–50.
9. H. Amani and M. Soltanieh: *Metall. Mater. Trans. B*, 2016, vol. 47 (4B), pp. 2524–34.
10. J.Z. Ashani and S.M. Bagheri: *Mater. Werkst.*, 2009, vol. 40, pp. 690–98.

11. D.M. Fronczek, J. Wojewoda-Budka, R. Chulist, A. Sypien, A. Korneva, Z. Szulc, N. Schell, and P. Zieba: *Mater. Design*, 2016, vol. 91, pp. 80–89.
12. N. Kahraman, B. Gülenç, and F. Findik: *Int. J. Imp. Eng.*, 2007, vol. 34, pp. 1423–32.
13. N. Kahraman and B. Gülenç: *J. Mater. Process. Tech.*, 2005, vol. 169, pp. 67–71.
14. R. Kaçar and M. Acarer: *J. Mater. Process. Tech.*, 2004, vol. 152, pp. 91–96.
15. W. Jiang, Y. Luo, G. Zhang, W. Woo, and S.T. Tu: *Mater. Design*, 2013, vol. 51, pp. 1052–59.
16. L.J. Zhang, Q. Pei, J.X. Zhang, Z.Y. Bi, and P.C. Li: *Mater. Design*, 2014, vol. 64, pp. 462–76.
17. R. Kaçar and M. Acarer: *Mater. Sci. Eng. A*, 2003, vol. 363, pp. 290–96.
18. Y. Kaya and N. Kahraman: *Mater. Design*, 2013, vol. 52, pp. 367–72.
19. M. Prazmowski, D. Rozumek, and H. Paul: *Eng. Fail. Anal.*, 2017, vol. 75, pp. 71–81.
20. Q. Chu, M. Zhang, J. Li, and C. Yan: *Mater. Sci. Eng. A*, 2017, vol. 689, pp. 323–31.
21. B. Wang, F. Xie, X. Luo, and J. Zhou: *J. Mater. Res. Tech.*, 2016, vol. 5 (4), pp. 333–38.
22. B. Gülenç, Y. Kaya, A. Durgutlu, İ.T. Gülenç, M.S. Yıldırım, and N. Kahraman: *Arch. Civil. Mech. Eng.*, 2016, vol. 16, pp. 1–8.
23. S. Belyaev, V. Rubanik, N. Resnina, V. Rubanik, Jr., E. Demidova, and I. Lomakin: *J. Mater. Process. Tech.*, 2016, vol. 234, pp. 323–31.
24. D.V. Lazurenko, I.A. Bataev, V.I. Mali, A.A. Bataev, I.N. Maliutina, V.S. Lozhkin, M.A. Esikov, and A.M.J. Jorge: *Mater. Design*, 2016, vol. 102, pp. 122–30.
25. G. Miao, H. Ma, Z. Shen, and Y. Yu: *Mater. Design*, 2014, vol. 63, pp. 538–43.
26. M. Acarer, B. Gülenç, and F. Findik: *J. Mater. Sci.*, 2004, vol. 39 (21), pp. 6457–66.
27. M. Acarer, B. Gülenç, and F. Findik: *Mater. Design*, 2003, vol. 24, pp. 659–64.
28. A.A. Akbari Mousavi and S.T.S. Al-Hassani: *J. Mech. Phys. Solids*, 2005, vol. 53, pp. 2501–28.
29. Y. Kaya: Ph D Thesis, Karabük University, TR, 2014, pp. 1–215.
30. W.F. Smith: *Structure and Properties of Engineering Alloys*, 2nd ed., McGraw-Hill Inc, New York, 1981.
31. N. Kahraman, B. Gülenç, and F. Findik: *J. Mater. Process. Tech.*, 2005, vol. 169, pp. 127–33.
32. M. Asemabadi, M. Sedighi, and M. Honarpisheh: *Mater. Sci. Eng. A*, 2012, vol. 558, pp. 144–49.
33. M.H. Bina, F. Dehghani, and M. Salimi: *Mater. Design*, 2013, vol. 45, pp. 504–09.
34. M. Yazdani, T.R. Toroghinejad, and S.M. Hashemi: *J. Mater. Eng. Perf.*, 2015, vol. 24, pp. 4032–43.
35. M.M.H. Athar and B. Tolaminejad: *Mater. Design*, 2015, vol. 86, pp. 516–25.
36. H.B. Xia, S.G. Wang, and H.F. Ben: *Mater. Design*, 2014, vol. 56, pp. 1014–19.
37. X. Guo, J. Tao, W. Wang, H. Li, and C. Wang: *Mater. Design*, 2013, vol. 49, pp. 116–22.
38. Y. Wang, H.G. Beom, M. Sun, and S. Lin: *Int. J. Imp. Eng.*, 2011, vol. 38, pp. 51–60.
39. T. Mooney: *ASM Handbook, Volume 13A-Corrosion: Fundamentals, Testing, and Protection*, ASM International, New York, 2003.
40. M. Acarer: *J. Mater. Eng. Perf.*, 2012, vol. 21 (11), pp. 2375–79.